


Parallelizable synthesis of arbitrary single-qubit gates with linear optics and time-frequency encoding

Antoine Henry ^{1,2}, Ravi Raghunathan,¹ Guillaume Ricard,^{1,3} Baptiste Lefaucher,¹ Filippo Miatto,¹ Nadia Belabas,² Isabelle Zaquine,¹ and Romain Alléaume^{1,3,*}

¹Télécom Paris-LTCl, Institut Polytechnique de Paris, 19 Place Marguerite Perey, 91120 Palaiseau, France

²Centre for Nanosciences and Nanotechnology, CNRS, Université Paris-Saclay, UMR 9001, 10 Boulevard Thomas Gobert, 91120 Palaiseau, France

³Curiosity Team, Inria Saclay, France



(Received 24 October 2022; revised 16 April 2023; accepted 8 June 2023; published 26 June 2023)

We propose methods for the exact synthesis of single-qubit unitaries with high success probability and gate fidelity, considering both time-bin and frequency-bin encodings. The proposed schemes are experimentally implementable with a spectral linear-optical quantum computation (S-LOQC) platform, composed of electro-optic phase modulators and phase-only programmable filters (pulse shapers). We assess the performances in terms of fidelity and probability of the two simplest three-component configurations for arbitrary gate generation in both encodings and give an exact analytical solution for the synthesis of an arbitrary single-qubit unitary in the time-bin encoding, using a single-tone rf driving of the electro-optic modulators. We further investigate the parallelization of arbitrary single-qubit gates over multiple qubits with a compact experimental setup, both for spectral and temporal encodings. We systematically evaluate and discuss the impact of the rf bandwidth, which conditions the number of tones driving the modulators, and of the choice of encoding for different targeted gates. We moreover quantify the number of high-fidelity Hadamard gates that can be synthesized in parallel, with minimal and increasing resources in terms of driving rf tones in a realistic system. Our analysis positions spectral S-LOQC as a promising platform to conduct massively parallel single-qubit operations, with potential applications to quantum metrology and quantum tomography.

DOI: [10.1103/PhysRevA.107.062610](https://doi.org/10.1103/PhysRevA.107.062610)

I. INTRODUCTION

Quantum information processing with light is a promising direction for near-term quantum computing. Quantum photonics systems are currently placed at the forefront of the technological race to engineer well-controlled optical quantum states in a Hilbert space of very high dimensionality, with a record value of 10^{43} [1]. Another key advantage of quantum photonics hardware is scalability based on photonic integration, now enabling compact photonic circuits approaching 1,000 components for millimeter-scale footprints [2].

A drawback of using light, however, is that photons do not interact with one another, which means that conditional operations need to be mediated by matter via some nonlinear process [3]. Even though nonlinear processes can theoretically implement the desired operations, this can lead in practice to very inefficient schemes, i.e., with very low probability of success. Linear optics quantum computation (LOQC), introduced in the pioneering work of Knill *et al.* in 2001 [4], performs universal quantum computing with light, using only linear optics and postselection. A different scheme, spectral linear-optical quantum computation (S-LOQC), was proposed [5] as a highly promising approach for scalable quantum information processing. S-LOQC harnesses photonic qubits encoded

over spectral modes (dual-rail frequency encoding) and gate transformations implemented with off-the-shelf telecom components: electro-optics modulators (EOM) and phase-only programmable filters (PS). S-LOQC notably leverages the spectral degrees of freedom that can allow to reach high dimensionality much more easily than spatial and polarization degrees of freedom. It can be used as a quantum frequency processor [6], to build high-dimensional quantum gates, with applications such as quantum process tomography or quantum networking at telecom wavelength.

The question of unitary gate synthesis in S-LOQC has already been studied in a series of work over the past few years. In the seminal paper [5], a setup comprising two PS [P] and two EOM [P] in the sequence [PEPE] was first considered. Using numerical optimization techniques, a deterministic Hadamard gate for spectral dual-rail encoding was theoretically designed with a unity fidelity and success. The question of parallelization was also studied, however it was found that a minimum of six modes separating two qubits was needed to ensure a success probability $>90\%$. The number of components, ancilla bits, and guard bands required were found to be higher for the synthesis of the controlled-Z (CZ) gate.

In Ref. [7], the authors adapted their scheme from Ref. [5] to experimentally implement high-fidelity frequency beam splitters and tritters with classical light. Two important modifications from their previous proposal involved reducing the

*romain.alleaume@telecom-paris.fr

number of components from four to three (in an [EPE] sequence) and the use of phase-shifted sine waves as the EOM rf driving, as opposed to arbitrary waveforms, which place greater demands on bandwidth. Using this [EPE] single-tone scheme, a beam splitter was experimentally realized with a fidelity of ~ 0.99998 and success probability $\sim 97.39\%$ at 1545.04 nm. The scheme was also shown to be well suited for parallelization, where the separation between adjacent beam splitters was found to be a minimum of four spectral modes, allowing for 33 beam splitters to be implemented in parallel under the constraints of the experiment. Furthermore, with the addition of an extra tone to the EOM rf driving, a frequency tritter with fidelity ~ 0.9989 and success probability $\sim 97.30\%$ was synthesized.

The same [EPE] scheme was then used to implement distinct quantum gates (Hadamard and identity) in parallel, in frequency-bin encoding [8]. The corresponding programmable unitary was moreover used to tune the overlap between adjacent spectral bins, which allowed to observe spectral Hong-Ou-Mandel interference with a visibility of 97%. More generally, it was shown that individual single-qubit gate operations can be applied in parallel to each of an ensemble of copropagating qubits, where each operation can be smoothly tuned between the identity and Hadamard gates.

More recently, arbitrary control of spectral qubits was reported in Ref. [9] with the same set of components [EPE], (i) experimentally with a single-tone sine wave modulation, and (ii) numerically for dual-tone modulation. The two-qubit controlled-NOT (CNOT) gate with the same setup ([EPE] and BFC source) [10] was also reported. Gate reconstruction was performed from measurements in the two-photon computational basis alone, and a fidelity $\mathcal{F} \approx 0.91$ was inferred.

In our work we explore S-LOQC further, with a focus on single-qubit unitary gate synthesis, first for a single qubit, and then for many qubits in parallel. S-LOQC is indeed naturally adapted for parallelization, allowing, without substantial change in the implementation, to apply the same unitary gate to many qubits in parallel. While being used in several quantum information protocols [11,12] time-bin encoding has not been as much explored as frequency encoding in the context of the spectral LOQC platform. It has, however, been proved to be efficient for several tasks in quantum information processing [13–16]. Similarly to frequency encoding, it offers the advantages of a high-dimensional accessible Hilbert space, and we show here that time encoding allows for more expressive gate synthesis possibilities than frequency encoding while using the same number of phase modulators and pulse-shaper components.

We investigate both [EPE] and [PEP] configurations of components, and show that both configurations can be used to efficiently perform any unitary transformation, with unity fidelity and success probability. In particular, we exhibit an analytical solution for the synthesis of an arbitrary single-qubit unitary using minimal resources, i.e., a single-tone rf driving for the EOM. Moreover, we also show that those transformations can be applied in parallel with time encoding to a larger number of qubits than what is possible with frequency encoding. We study, for several gates, the trade-off between the quality (fidelity, success probability) of the synthesis, the

parallelization that can be achieved, and the resources needed, in particular in terms of rf bandwidth.

The article is organized as follows: we introduce in Sec. II the formalism for encoding both in time or frequency basis and for the corresponding Hilbert spaces, and the description of the components in both bases. Section III defines the general problem of qubit unitary gate synthesis that we tackle in this article and explains the rationale of our approach. We notably detail the two-scattering model for the pulse shaper in the time basis, that will be instrumental for the results reported in Sec. IV. We finally detail how the performance parameters for gate synthesis, namely, fidelity and success probability, are defined. The next two sections report our results, which consist in a systematic and wide exploration of the different options, in terms of encoding bases, gates, and configurations (either [EPE] or [PEP]). Section IV presents our results related to the synthesis unitary gates, for a single qubit. Remarkably, we exhibit, in the time basis, an exact solution allowing the synthesis of an arbitrary single-qubit unitary with single-tone rf driving of the EOM, in both [EPE] and [PEP] configurations. These results are put in perspective with single-qubit unitary gate synthesis in the frequency basis, whose fidelity and success probability depend on the type of gate that is targeted. Section V then presents our results related to the parallel synthesis of the same qubit gate over many different qubits. Here again, we compare the two encodings, as well as the two considered configurations, and discuss the interplay between the performance of the synthesis and the number of rf tones.

II. TIME AND FREQUENCY FORMALISM FOR S-LOQC

In this section we define the photonic states that we will employ and the theoretical description of the pulse shaper (PS) and the EOM. The descriptions of the devices must take into account the EOM and PS physical characteristics, as these characteristics set a limit on the total number of available modes for quantum manipulation.

A. Optical modes and quantum states

The system that we consider is composed of M optical modes identified either by a frequency bin of width $\delta\omega$, centered on ω_j , or by a time bin of width δt , centered on t_k . Frequency modes $|\omega_j\rangle$ are linear combinations of time-bin modes $|t_k\rangle$. These two sets of basis vectors are connected by a discrete Fourier transform

$$|t_k\rangle \approx \frac{1}{\sqrt{M}} \sum_{j=0}^{M-1} \exp\left(i\frac{2\pi}{M}jk\right) |\omega_j\rangle, \quad (1)$$

$$|\omega_j\rangle \approx \frac{1}{\sqrt{M}} \sum_{k=0}^{M-1} \exp\left(-i\frac{2\pi}{M}jk\right) |t_k\rangle. \quad (2)$$

The interchange between the frequency and time bases is exact only in the continuous case, when $M \rightarrow \infty$ and $\delta\omega, \delta t \rightarrow 0$.

To operate on single qubits, we divide our Hilbert space of dimension M into $M/2$ independent subspaces according to a choice of qubit encoding either in the frequency

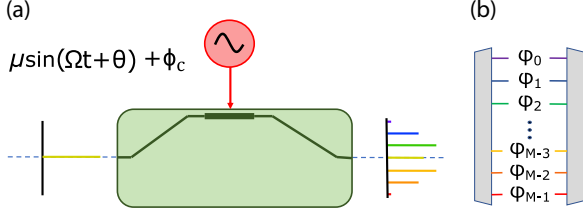


FIG. 1. Action of (a) the electro-optic phase modulator and (b) the pulse shaper in the frequency basis.

domain \mathcal{H}_j^ω using two contiguous frequency bins or in the time domain \mathcal{H}_k^t using modes separated by $M/2$ time bins, with $j, k \in [0, M/2 - 1]$.

$$\mathcal{H}_j^\omega = \{|\omega_{2j}\rangle, |\omega_{2j+1}\rangle\}, \quad \omega_{2j+1} - \omega_{2j} = \delta\omega, \quad (3)$$

$$\mathcal{H}_k^t = \{|t_k\rangle, |t_{k+M/2}\rangle\}, \quad t_{k+M/2} - t_k = \frac{M}{2}\delta t, \quad (4)$$

Such a qubit encoding choice is made to take into account the technical limitations of the devices. In the present case, the fact that the EOM couples mainly neighboring frequency modes justifies the choice of adjacent modes to encode frequency-bin qubits. Conversely, the fact that the PS couples time modes that are $M/2$ time bins apart (cf. Appendix B) justifies the choice of encoding used for the time-bin qubits.

As the considered Hilbert spaces are orthogonal, we can write the sum of the subspaces as

$$\mathcal{H} = \bigoplus_j \mathcal{H}_j^\omega = \bigoplus_k \mathcal{H}_k^t. \quad (5)$$

We now introduce the devices that we are using for photonic qubit processing.

B. Pulse shaper

The PS can shift the phase of frequency modes concurrently and independently. It is therefore characterized by a set of M angles $\{\varphi_j\}$ (one angle per mode) that can be chosen freely, without constraints. In general, the PS acts as the tensor product of distinct phase shifts operators, one per frequency mode, and its operator \hat{U}_{PS} can be written

$$\hat{U}_{\text{PS}} = \bigotimes_{j=0}^{M-1} \exp(i\varphi_j \hat{N}_{\omega_j}), \quad (6)$$

where \hat{N}_{ω_j} is the number operator of the ω_j frequency mode: $\hat{N}_{\omega_j} = \sum_n n |n_{\omega_j}\rangle \langle n_{\omega_j}|$. However, in the restricted case of a single photon, we can thus treat the PS as a diagonal matrix P in the frequency basis. Its action on the one-photon subspace is described in Fig. 1(b).

$$P|\omega_j\rangle = e^{i\varphi_j} |\omega_j\rangle. \quad (7)$$

In order to describe the action of the PS in the time basis (see Fig. 2), we use the Fourier transform $\tilde{P} = FPF^\dagger$, where the matrix F and the detailed calculations are given in Appendix A, and we obtain

$$\tilde{P}|t_k\rangle = \frac{1}{M} \sum_{k'=0}^{M-1} \sum_{j=0}^{M-1} \exp\left(i\frac{2\pi}{M}(k' - k)j + \varphi_j\right) |t_{k'}\rangle. \quad (8)$$

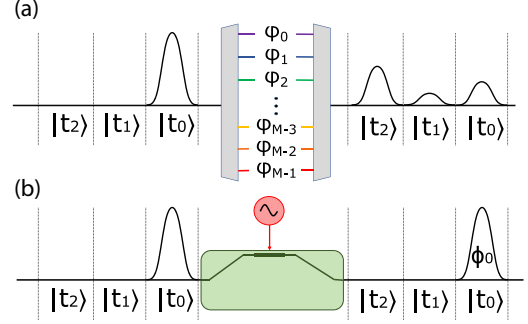


FIG. 2. Action of the (a) pulse shaper and (b) electro-optic phase modulator in the time basis.

The PS is therefore a scatterer in the time basis, coupling a single time mode to all the other modes. The number of modes over which a single mode can be scattered will be an important optimization parameter, as shown in Sec. III C 1.

C. EOM

The EOM is a device that is complementary to the PS as it performs phase shifts of individual modes in the time domain, and therefore its operator can be expressed as

$$\hat{U}_{\text{EOM}} = \bigotimes_{k=0}^{M-1} \exp(i\phi_k \hat{N}_{t_k}), \quad (9)$$

where \hat{N}_{t_k} is the number operator of the t_k time-bin mode: $\hat{N}_{t_k} = \sum_n n |n_{t_k}\rangle \langle n_{t_k}|$. Within our restriction to the one-photon subspace, we can write the action of the EOM over time modes $|t_k\rangle$ as a diagonal matrix E in the $\{|t_k\rangle\}$ basis as

$$E|t_k\rangle = e^{i\phi_k} |t_k\rangle. \quad (10)$$

Contrary to the PS case, the set of angles $\{\phi_k\}$ for the EOM cannot be chosen freely. It is determined by the rf driving. For instance, in the case of a monochromatic (or single-tone) rf driving, the phase ϕ_k applied to the optical wave can be written as a sinusoidal function of time with frequency Ω

$$\phi_k = \mu \sin(\Omega t_k + \theta) + \phi_c, \quad (11)$$

with $\mu = \pi \frac{V_m}{V_\pi}$ the modulation index proportional to the modulation amplitude V_m and V_π the half-wave voltage of the EOM, $\theta \in [0, \pi]$ a constant angle, and $\phi_c \in [0, \pi]$ a constant phase shift applied to all time bins. In practice, μ is limited by the power of the rf source that drives the EOM (typically μ is of order 1), and by the EOM characteristics. The maximum frequency Ω is determined by the frequency response of the EOM.

We can describe the action of the EOM in the frequency basis [17,18] (see Fig. 1) through the Fourier transform $\tilde{E} = FEF^\dagger$ and check that the EOM creates left- and right-side bands (spaced by Ω) with amplitude decreasing according to Bessel functions. If the mode spacing $\delta\omega$ is set equal to the rf driving single-tone Ω , we have

$$\tilde{E}|\omega_j\rangle = e^{i\phi_c} \sum_{k=-\lceil\mu\rceil-1}^{k=\lceil\mu\rceil+1} (e^{i\theta})^k J_k(\mu) |\omega_{j+k}\rangle. \quad (12)$$

The sum can be extended to $\pm\infty$ as the additional terms are weighed by vanishing Bessel functions [19].

The EOM is therefore a scatterer in the frequency basis.

D. Orders of magnitude

The PS and the EOM act on conjugate variables (frequency and time), which are related by a Fourier transform, which results in relationships between bandwidths and resolutions. We denominate $\Delta\omega$ and $\delta\omega$, respectively, as the total frequency bandwidth that the PS can operate on and its frequency resolution. On the other hand, if the EOM is driven at a rf Ω , it can generate sidebands at intervals Ω . This naturally defines a number $M_\omega = \Delta\omega/\Omega$ frequency modes as long as $\delta\omega \lesssim \Omega$, so that the PS can distinguish and address them individually. It is important to match the number of frequency modes and time modes to make sure that the two devices are acting on two conjugate bases of the same Hilbert space.

In the time domain, the resolution δt will be limited by the characteristic times of the detectors. The period of the rf driving the EOM is $T = 2\pi/\Omega$, which in principle defines $M_t = T/\delta t = \Delta\omega/\Omega = M_\omega$ time modes.

A realistic PS (Finisar WaveShaper 4000A) has a total bandwidth $\Delta\omega = 5.36$ THz, and the rf voltage signal that drives the EOM can be set to be a sine wave with a frequency in the order of 10 GHz (which is close to the frequency resolution of the PS). From these figures we derived a number of time and frequency modes $M = T/\delta t = \Delta\omega/\delta\omega \approx 536$, and in our calculations, we chose $M = 2^7 = 128$ modes.

III. PROBLEM DEFINITION: QUBIT GATE SYNTHESIS WITH EOM AND PS

A. Objective

Our aim is to synthesize single-qubit quantum gates using some combination of the components described in the previous section, namely, PS and EOM. A single-qubit gate is by definition a unitary transformation over a two-dimensional Hilbert space, and is hence represented by a 2×2 unitary matrix, whereas the components can be described by unitaries (P , \tilde{P} , E , and \tilde{E}) that can operate over a much larger, M -dimensional Hilbert space. Describing how to perform single-qubit gate synthesis in this context therefore requires specifying several types of information:

(1) The configuration, i.e., how many components are combined into the unitary. After justifying that the minimum number of components is three, we focus in this article on two main configurations, [EPE] and [PEP].

(2) The values of the different components free parameters, (phases of the form $\varphi_0, \dots, \varphi_{M-1}$ for the pulse shaper, and parameters μ, θ, ϕ_c for an electro-optic modulator driven with a single frequency modulation at Ω).

(3) The choice of encoding, i.e., a choice of two orthonormal M -dimensional vectors, $\{|e_1\rangle, |e_2\rangle\}$, that constitute the encoding basis and are identified with the logical qubit basis $\{|0_L\rangle, |1_L\rangle\}$.

As explained in the previous section, we will use both frequency basis $\{|\omega_i\rangle, |\omega_j\rangle\}$ and time basis $\{|t_i\rangle, |t_j\rangle\}$ as defined in Eqs. (3) and (4).

B. Performance metrics

For a given configuration (e.g., combination of PS and EOM), we can define a global operator $\hat{V}(\Phi)$ and the corresponding $M \times M$ unitary matrix $V(\Phi)$, product of n PS and n' EOM, depending on many parameters that we will globally denote as $\Phi \equiv (\varphi_{1,0}, \dots, \varphi_{n,M-1}, \mu_{1,0}, \theta_{1,0}, \phi_{c_{1,0}}, \dots, \mu_{n',M-1}, \theta_{n',M-1}, \phi_{c_{n',M-1}})$.

The choice of the encoding $\{|e_1\rangle, |e_2\rangle\} \leftrightarrow \{|0_L\rangle, |1_L\rangle\}$ then directly induces a reduced 2×2 matrix $W(\Phi)$ defined as

$$W(\Phi) = \begin{pmatrix} \langle 0_L | \hat{V}(\Phi) | 0_L \rangle & \langle 0_L | \hat{V}(\Phi) | 1_L \rangle \\ \langle 1_L | \hat{V}(\Phi) | 0_L \rangle & \langle 1_L | \hat{V}(\Phi) | 1_L \rangle \end{pmatrix}. \quad (13)$$

If T represents the (ideal) target qubit unitary that one wants to synthesize, then the performance of the synthesis can be quantified by comparing this resultant 2×2 matrix $W(\Phi)$ to the target (ideal) gate T . The performance of the synthesis can be essentially captured by two parameters:

(1) The success probability \mathcal{P} , which measures the stability of the two-dimensional subspace $\{|e_1\rangle, |e_2\rangle\}$, under the unitary $V(\Phi)$,

$$\mathcal{P}(W, T) = \frac{\text{Tr}(W^\dagger W)}{\text{Tr}(T^\dagger T)}; \quad (14)$$

(2) The fidelity \mathcal{F} , which measures the accuracy of the synthesis of the target single-qubit gate (in other words, it measures how close we are to the gate we intended to synthesize in the first place),

$$\mathcal{F}(W, T) = \frac{\text{Tr}(W^\dagger T) \text{Tr}(T^\dagger W)}{\text{Tr}(W^\dagger W) \text{Tr}(T^\dagger T)}. \quad (15)$$

C. Arbitrary unitary synthesis for a single qubit

We will identify configurations of components, and encoding methods for which it is possible to synthesize any single-qubit unitary, by varying the free parameters of Φ , and this with fidelity and success probability greater than some given threshold values, which we denote \mathcal{F}_{th} and \mathcal{P}_{th} . This objective is captured in the following definition:

For a given encoding $\{|e_1\rangle, |e_2\rangle\} \leftrightarrow \{|0_L\rangle, |1_L\rangle\}$, a configuration $\hat{V}(\Phi)$ can perform arbitrary single-qubit unitary synthesis with precision \mathcal{F}_{th} , \mathcal{P}_{th} if $\forall U \in SU(2)$, $\exists \Phi$ such that $\mathcal{P}(W(\Phi), U) \geq \mathcal{P}_{th}$ and $\mathcal{F}(W(\Phi), U) \geq \mathcal{F}_{th}$.

An arbitrary unitary matrix can be described with four parameters,

$$\mathcal{M}(a, b, c, d) = e^{ia} \begin{pmatrix} \cos\left(\frac{c}{2}\right) e^{-i\left(\frac{b}{2} + \frac{d}{2}\right)} & -\sin\left(\frac{c}{2}\right) e^{-i\left(\frac{b}{2} - \frac{d}{2}\right)} \\ \sin\left(\frac{c}{2}\right) e^{i\left(\frac{b}{2} - \frac{d}{2}\right)} & \cos\left(\frac{c}{2}\right) e^{i\left(\frac{b}{2} + \frac{d}{2}\right)} \end{pmatrix}, \quad (16)$$

where $a, b, c, d \in \mathbb{R}$. Note that if an arbitrary single-qubit unitary synthesis is achieved with $\mathcal{F} = 1$ and $\mathcal{P} = 1$ with a given configuration and some encoding, then any other basis choice within the subspace $\{|e_1\rangle, |e_2\rangle\}$ will lead to an arbitrary single-qubit synthesis as the change of encoding is a unitary operation. On the other hand, if a configuration cannot achieve arbitrary synthesis, then the ability to synthesize one given target gate U will vary with the basis choice.

1. Subspace stability and choice of encoding

We aim in general at the highest possible \mathcal{F} and \mathcal{P} for every gate synthesis. The requirement on the success probability \mathcal{P} can be used as a guideline for the choice of the encoding basis we consider. A necessary condition to achieve a high success probability is to pick an encoding subspace that is (approximately) stable under the action of $\hat{V}(\phi)$. From the previous considerations on the pulse shaper and the electro-optic phase modulator, we get a first intuition on the difficulties of obtaining some transformations, according to the considered encoding: some require energy exchange between the two basis states, as, for instance, the X or Y Pauli transformations, whereas some only require phase changes, such as the Z Pauli transformation. A very important example is that of the Hadamard transformation that achieves the balanced splitting of the energy between the two modes corresponding to the basis states. It is therefore important to choose the component combination and encoding in order to be able to control both phase changes and energy exchanges between the two modes of the computational basis. In any component combination, we need either a dephasing element, a scatterer, or a certain combination of these two elements. The stability condition will be satisfied if the combination of components and the encoding allow the scattered energy to remain in the subspace defining the qubit. Let us now consider the consequence of this requirement, for our two families of encoding.

(a) *Frequency encoding.* In the frequency basis, all vectors are stable under the action of the pulse shaper but the EOM acts as a scatterer. The number of modes where the energy is scattered from one given initial mode depends on the modulation index. As mentioned, because the EOM couples frequency modes locally [see Eq. (12) and Fig. 1], the computational basis is formed of adjacent modes of the form $\{|\omega_i\rangle, |\omega_i + 1\rangle\}$ when studying synthesis in the frequency encoding as in Ref. [5].

(b) *Time encoding.* In the time basis, all vectors are stable under the action of the EOM but the PS acts as a scatterer. The large number of independent parameters available for the PS allows a variety of scattering possibilities.

Proposition 1. PS parameters can be chosen to satisfy the two-scattering assumption

$$\forall k \in [0, M/2 - 1], \quad \tilde{P}|t_k\rangle = \alpha|t_k\rangle + \beta|t_{k+M/2}\rangle,$$

where α and β are complex numbers, linked by the unitarity condition $|\alpha|^2 + |\beta|^2 = 1$. This ensures the stability of our time qubit subspace in all transformations including PS and EOM when using the basis choice $\{|0_L\rangle = |t_k\rangle, |1_L\rangle = |t_{k+M/2}\rangle\}$.

In Appendix B we calculate the PS parameters that allow to satisfy the two-scattering assumption and we derive the matrix elements of the PS both in the frequency basis and in the time basis

$$P|\omega_j\rangle = [\alpha + \beta e^{-i2\pi m \frac{j}{M}}]|\omega_j\rangle. \quad (17)$$

We obtain

$$\forall k \in \left[0, \frac{M}{2} - 1\right], \quad \tilde{P}|t_k\rangle = \alpha|t_k\rangle + \beta|t_{k+M/2}\rangle$$

$$\forall k \in \left[\frac{M}{2} - 1, M - 1\right], \quad \tilde{P}|t_k\rangle = \beta|t_k\rangle + \alpha|t_{k-M/2}\rangle. \quad (18)$$

The matrix in the time basis is therefore

$$\tilde{P} = e^{i\gamma} \begin{pmatrix} |\alpha|I_{\frac{M}{2}} & \pm i|\beta|I_{\frac{M}{2}} \\ \pm i|\beta|I_{\frac{M}{2}} & |\alpha|I_{\frac{M}{2}} \end{pmatrix}, \quad (19)$$

where $I_{\frac{M}{2}}$ stands for an identity matrix of dimension $M/2$ and γ is a global phase induced by the pulse shaper. When using the basis choice $\{|0_L\rangle = |t_k\rangle, |1_L\rangle = |t_{k+M/2}\rangle\}$, the 2×2 matrix of the PS can be mapped to the matrix of a rotation of angle θ_{PS} about the x axis in the Bloch sphere, with

$$e^{i\gamma}|\alpha\rangle = \cos \frac{\theta_{\text{PS}}}{2};$$

$$e^{i\gamma}|\beta\rangle = \sin \frac{\theta_{\text{PS}}}{2}. \quad (20)$$

It can also be mapped to the matrix of an arbitrary beam splitter with reflexion and transmission coefficients r and t ,

$$|\alpha\rangle = |r\rangle$$

$$|\beta\rangle = |t\rangle. \quad (21)$$

In the same way, the matrix of the EOM in the time basis can be written

$$E = e^{i\phi_c} \begin{pmatrix} \text{diag}\{e^{\phi_k}\}_{0 \leq k \leq \frac{M}{2}-1} & 0 \\ 0 & \text{diag}\{e^{-\phi_k}\}_{0 \leq k \leq \frac{M}{2}-1} \end{pmatrix}. \quad (22)$$

With the chosen encoding, the 2×2 matrix of the EOM can be identified to the matrix of a rotation of angle θ_{EOM} about the z axis in the Bloch sphere, with

$$i\phi_c + \phi_k = -i\theta_{\text{EOM}}/2$$

$$i\phi_c - \phi_k = i\theta_{\text{EOM}}/2. \quad (23)$$

2. Minimum number of components

Using the analogy with rotations and the fact that an arbitrary unitary transformation requires the composition of three rotations about two orthogonal axes of the Bloch sphere [20], we derive that a minimum number of three components will be required to synthesize an arbitrary unitary transformation, using pulse shapers and electro-optic phase modulators. Since two EOM or two PS in serial are equivalent to one, the sequences with minimum resource to investigate are [EPE] and [PEP]. We investigate the case of the single qubit for both frequency and time bases encoding.

IV. RESULTS FOR SINGLE-QUBIT GATE SYNTHESIS

A. Frequency encoding

Within each frequency subspace, we define the logical basis as

$$|0_L\rangle_j = |\omega_j\rangle \quad |1_L\rangle_j = |\omega_{j+1}\rangle. \quad (24)$$

1. [EPE] configuration

This configuration has been thoroughly investigated [5,7–10] and the theoretical results about one-qubit gates synthesis

are summarized in Table I. Experimental implementation of Hadamard have been reported in Ref. [7], the control-NOT gate in Ref. [10], and more recently arbitrary transformations of a single qubit in Ref. [9]. The limitation on success probability arises from the difficulty to control the scattering of energy in many modes by the EOM. This is also the reason why guard bands must be used to avoid crosstalk when working with qubits in parallel in the frequency domain: the

coupling to adjacent modes cannot be perfectly controlled, even with ideal lossless devices.

2. [PEP] configuration

In order to assess this configuration, the first step is to write the generic element of the corresponding synthesized matrix, using two diagonal matrices P_1 and P_2 for the PS and Eq. (12) for the EOM matrix \tilde{E} in the frequency basis

$$\forall k, k' \in [0, M-1], (P_2 \tilde{E} P_1)_{k'k} = e^{i(\varphi_{1,k} + \varphi_{2,k'} + \phi_c)} \sum_{k=k'-\lceil\mu\rceil-1}^{k=k'+\lceil\mu\rceil+1} (e^{i\theta})^{k'-k} J_k(\mu). \quad (25)$$

For qubit j , $\forall j \in [0, M/2-1]$ encoded over modes $|\omega_j\rangle$ and $|\omega_{j+1}\rangle$, the matrix of the synthesized unitary is given by

$$\mathbf{W}_j = e^{i\phi_c} \begin{pmatrix} J_0(\mu) e^{i(\varphi_{1,2j} + \varphi_{2,2j})} & e^{-i\theta} J_1(\mu) e^{i(\varphi_{1,2j+1} + \varphi_{2,2j})} \\ -e^{i\theta} J_1(\mu) e^{i(\varphi_{1,2j} + \varphi_{2,2j+1})} & J_0(\mu) e^{i(\varphi_{1,2j+1} + \varphi_{2,2j+1})} \end{pmatrix}, \quad (26)$$

where $\varphi_{n,m}$ is the phase applied by PS_n to mode m .

Let $\mathcal{M}(a, b, c, d)$ be the matrix of an arbitrary unitary as given in Eq. (16). One can achieve an exact synthesis of U over qubit j if parameters φ match the following set of conditions:

$$\begin{cases} J_0(\mu) = \cos(c/2) \\ J_1(\mu) = \sin(c/2) \end{cases} \begin{cases} \varphi_{1,2j} = \frac{-d-\theta+\pi+s_j}{2} \pmod{\pi} \\ \varphi_{2,2j} = -\frac{b+d}{2} + \varphi_{1,2j} \pmod{\pi} \\ \varphi_{1,2j+1} = s_j - \varphi_{1,2j} \pmod{\pi} \\ \varphi_{2,2j+1} = -s_j + \left(\frac{b-d}{2} + \varphi_{1,2j}\right) \pmod{\pi}. \end{cases} \quad (27)$$

If the parameters of the pulse shapers satisfy the second set of equations, then fidelity and success probability do not depend on the qubit number j and are given by

$$\mathcal{P} = J_0(\mu)^2 + J_1(\mu)^2, \quad (28)$$

$$\mathcal{F} = \frac{[J_0(\mu) \cos(\frac{c}{2}) + J_1(\mu) \sin(\frac{c}{2})]^2}{J_0(\mu)^2 + J_1(\mu)^2}. \quad (29)$$

TABLE I. Comparison of the success probabilities of single-qubit arbitrary unitary synthesis with [EPE] and [PEP] configurations for single-tone driving at Ω of the EOM and for two encodings, with unit fidelities. The bold part corresponds to results reported in this work.

Arbitrary unitary synthesis for a single qubit		
Config.	Frequency encoding $\{ \omega_j\rangle, \omega_{j+1}\rangle\}$	Time encoding $\{ t_k\rangle, t_{k+M/2}\rangle\}$
[EPE]		
Driving at Ω	Phase gate : $\mathcal{F} = 1, \mathcal{P} = 1$ H gate : $\mathcal{F} = 1, \mathcal{P} = 0.98$ Flip gate : $\mathcal{F} = 1, \mathcal{P} = 0.81$	$\mathcal{F} = 1, \mathcal{P} = 1$ \forall gates (See Prop. 2)
[PEP]		
Driving at Ω	Phase gate : $\mathcal{F} = 1, \mathcal{P} = 1$ H gate : $\mathcal{F} = 1, \mathcal{P} = 0.60$ Flip gate : $\mathcal{F} = 1, \mathcal{P} = 0.27$	$\mathcal{F} = 1, \mathcal{P} = 1$ \forall gates (See Prop. 3)

Subsequently, we get the following results on the best achievable performances of the [PEP] configuration, indicating that unit success probability and unit fidelity can only be obtained for phase gates.

$$\mathcal{P} = 1 \Leftrightarrow \mu = 0$$

$$\mathcal{F} = 1 \Leftrightarrow J_0(\mu) \sin\left(\frac{c}{2}\right) = J_1(\mu) \cos\left(\frac{c}{2}\right) \quad (30)$$

$$\mathcal{P} = \mathcal{F} = 1 \Leftrightarrow \mu = c = 0.$$

Figure 3 summarizes the performance of gate synthesis for this configuration. Varying μ allows to cover all unitaries. The dephasing applied to each frequency mode by the pulse shapers are chosen such that $\mathcal{F} = 1$ is achievable for all gates but with a decreasing success probability \mathcal{P} . The bit flip gate

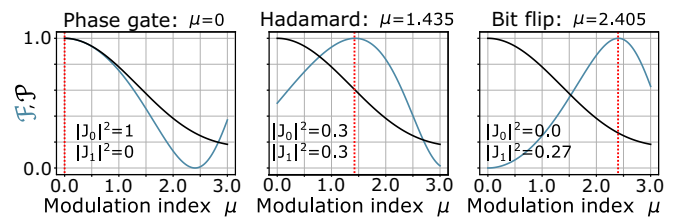


FIG. 3. Success probability \mathcal{P} (black line) and fidelity \mathcal{F} (blue line) for phase, Hadamard, and X (bit flip) gates in the [PEP] configuration for frequency-bin qubits as functions of the modulation index of E, μ . Varying μ covers all angles θ of the Bloch sphere following Eq. (26). The performance of the gate does not depend on the rotation around the z axis.

X appears, for this configuration, as the worst case in terms of gate synthesis objective: it is the gate for which the success probability, conditioned on unit fidelity, is the lowest.

We can see some intrinsic limitation of the frequency encoding, when using the [PEP] configuration, due to the loss of energy in the side bands induced by the EOM. The gates requiring no coupling or energy exchange between the two modes of the qubit (phase gates) exhibit unity success probability, as all the energy remains in the computational modes. For the other gates, however, the more coupling we need, the greater the index of modulation, and the more energy gets lost in the adjacent modes, leading to a lower success probability. In summary, the success probability in this case is lower than in the previous configuration, especially for the X gate: with only one EOM, the energy scattered in adjacent modes cannot be coupled back to the qubit subspace.

A heuristic justification that multiple tones do not bring improvement in the parallel synthesis of single qubit gates, in the PEP configuration, and for frequency encoding, lies in the fact that more tones will lead to more scattering out of the computational space, and hence a decrease of the success probability of the gate.

This [PEP] configuration has been used with spectral encoding implementing Hadamard gates for quantum state tomography and probabilistic Hong-Ou-Mandel [21–25]. [PEP] configuration has not been explored up to now for arbitrary gate synthesis. We can note that the dephasing action of a pulse shaper acting on two frequency modes could also be obtained by adjusting a linearly dispersive optical delay, and

hence emulate [PEP] by [E + delay lines]. On the other hand, the use of pulse shapers is necessary to handle many frequency qubits in parallel.

B. Time encoding

In this basis, the matrices of the two components are

$$\begin{aligned} \tilde{P} &= e^{i\gamma} \begin{pmatrix} |\alpha|I & \pm i|\beta|I \\ \pm i|\beta|I & |\alpha|I \end{pmatrix}; \\ E &= e^{i\phi_c} \begin{pmatrix} \text{diag}\{e^{i\phi_k}\}_{0 \leq k \leq \frac{M}{2}-1} & 0 \\ 0 & \text{diag}\{e^{-i\phi_k}\}_{0 \leq k \leq \frac{M}{2}-1} \end{pmatrix}. \end{aligned} \quad (31)$$

The qubit is encoded over two time modes separated by $M/2$ modes

$$|0_L\rangle_k = |t_k\rangle \quad |1_L\rangle_k = |t_{k+M/2}\rangle. \quad (32)$$

1. [EPE] configuration

Proposition 2. One can achieve exact synthesis of any single qubit arbitrary unitary U with a single-frequency rf driving with the [EPE] configuration.

Proof. Let α , β , and γ be the parameters of the pulse shaper in the time basis, μ_i , θ_i the parameters of the EOM_i ($i \in \{1, 2\}$), and $\mathcal{M}(a, b, c, d)$ the matrix of an arbitrary unitary U . We consider qubit $k \in [0, M/2 - 1]$ encoded on modes $|t_k\rangle$ and $|t_{k+M/2}\rangle$. The matrix of the three-component configuration is

$$V = E_2 \tilde{P} E_1 = e^{i(\phi_{c,1} + \phi_{c,2} + \gamma)} \begin{pmatrix} |\alpha| \text{diag}\{e^{i(\phi_{1,k} + \phi_{2,k})}\} & \pm i|\beta| \text{diag}\{e^{i(-\phi_{1,k} + \phi_{2,k})}\} \\ \pm i|\beta| \text{diag}\{e^{i(\phi_{1,k} - \phi_{2,k})}\} & |\alpha| \text{diag}\{e^{-i(\phi_{1,k} + \phi_{2,k})}\} \end{pmatrix}, \quad (33)$$

which yields the matrix of the synthesized unitary for the qubit encoded over modes $|t_k\rangle$ and $|t_{k+M/2}\rangle$,

$$\forall k \in [0, M/2 - 1], \mathbf{W}_k = e^{i(\phi_{c,1} + \phi_{c,2} + \gamma)} \begin{pmatrix} |\alpha| e^{i(\phi_{1,k} + \phi_{2,k})} & \pm i|\beta| e^{i(-\phi_{1,k} + \phi_{2,k})} \\ \pm i|\beta| e^{i(\phi_{1,k} - \phi_{2,k})} & |\alpha| e^{-i(\phi_{1,k} + \phi_{2,k})} \end{pmatrix}. \quad (34)$$

Identification with $\mathcal{M}(a, b, c, d)$ yields the following set of conditions for qubit k :

$$\begin{cases} |\alpha| = \cos(c/2) \\ |\beta| = \sin(c/2) \end{cases} \begin{cases} \phi_{1,k} + \phi_{2,k} = \frac{-b-d}{2} \pmod{2\pi} \\ -\phi_{1,k} + \phi_{2,k} + \pi/2 = \frac{-b+d}{2} + \pi \pmod{2\pi} \\ \phi_{1,k} - \phi_{2,k} + \pi/2 = \frac{b-d}{2} \pmod{2\pi} \\ -\phi_{1,k} - \phi_{2,k} = \frac{b+d}{2} \pmod{2\pi}, \end{cases} \quad (35)$$

which finally gives

$$\begin{aligned} |\alpha| &= \cos(c/2); & |\beta| &= \sin(c/2) \\ \phi_{1,k} &= \frac{-d}{2} - \pi/4 \pmod{\pi} \\ \phi_{2,k} &= \frac{-b}{2} + \pi/4 \pmod{\pi}. \end{aligned} \quad (36)$$

As we consider a sinusoidal rf driving, the dephasing applied by the EOM to each temporal mode $|t_k\rangle$ is $\phi_k = \mu \sin(\frac{2k\pi}{M} + \theta)$, ($\forall k \in \llbracket 0, M/2 - 1 \rrbracket$), which gives

$$\begin{aligned} \phi_{1,k} &= \mu_1 \sin\left(\frac{2k\pi}{M} + \theta_1\right) = -\frac{d}{2} - \frac{\pi}{4} \pmod{\pi} \\ \phi_{2,k} &= \mu_2 \sin\left(\frac{2k\pi}{M} + \theta_2\right) = -\frac{b}{2} + \frac{\pi}{4} \pmod{\pi}. \end{aligned} \quad (37)$$

$$|\alpha| = \cos(c/2); \quad |\beta| = \sin(c/2); \quad \text{with } c \in [0, \pi]$$

The condition is satisfied with the following parameters:

$$\mu_1 = \frac{-\frac{d}{2} - \frac{\pi}{4}}{\sin\left(\frac{2k\pi}{M} + \theta_1\right)}; \quad \mu_2 = \frac{-\frac{b}{2} + \frac{\pi}{4}}{\sin\left(\frac{2k\pi}{M} + \theta_2\right)}$$

$$\theta_1, \theta_2 \neq -\frac{2k\pi}{M}. \quad (38)$$

This possibility of synthesizing an arbitrary unitary for a single qubit with unit success probability and fidelity is a noticeable advantage of the time encoding as compared to the frequency encoding for which only phase gates can exhibit such performance. ■

2. [PEP] configuration

Proposition 3. One can achieve an exact synthesis of an arbitrary unitary U over qubit k with a single-frequency rf driving with the [PEP] configuration.

Proof. Based on the two-scattering property demonstrated in Sec. III C 1, we can see the PS acts as a beam splitter in the time basis. The following EOM can then introduce an arbitrary phase shift between the two modes of the qubit subspace, while the final PS of this configuration acts as a second arbitrary beam splitter, completing a Mach-Zehnder interferometric device. Such Mach-Zehnder has been shown to achieve arbitrary unitary qubit synthesis [26]. ■

3. Trivial gates

It is noticeable that some gates do not require the three-component configuration. For instance, in the time basis, phase gates only require one EOM and no PS. X gates that do not even require any EOM can be trivially obtained in both [EPE] and [PEP] configurations. They correspond to the parameters $b = -d = \frac{\pi}{2}$ and the performances do not depend on the qubit number k , which means that they will also be trivially parallelized to all qubits. The whole family of bit flip gates requires only one PS and one EOM.

V. PARALLELIZATION OF QUBIT GATE SYNTHESIS

In this section, taking advantage of the possibility to address and manipulate a large number of modes with the same components E and P, we tackle the question of gate synthesis parallelization. More precisely, we explore the ability to parallelize the synthesis of an arbitrary single-qubit unitary, so that the same unitary can be applied to multiple qubits in parallel. We will moreover study the trade-offs between performance and the number of qubits on which the synthesis can be performed in parallel, both for frequency and time encodings and for the two three-component configurations, i.e., [EPE] and [PEP].

A. Frequency encoding

In the frequency basis, a qubit is encoded over two adjacent modes. Because the EOM inevitably scatters energy in the adjacent modes, using all the available frequency modes to encode quantum information would generate crosstalk problems. Considering a gate implemented with a single photon and considering its computational space and a mode outside

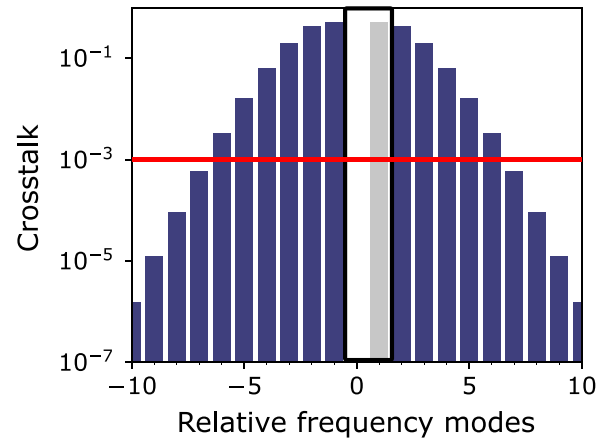


FIG. 4. Simulation of scattering probability for one photon injected in mode 0 and an X gate implemented on frequency modes 0 and 1. The parameters for the flip gate are given in Fig. 3. The computational space is indicated by the thick dark line. Starting with one photon in mode 0, the probability of finding one photon in the original mode 0 after the X gate is 3.99×10^{-9} , while the probability to have to have one photon in mode 1 is 27%. The red line indicates the threshold of 10^{-3} that is reached beyond six guard modes.

this space, we define crosstalk between the computational space and this outside mode as the probability of finding the photon in this outside mode after implementing the gate. We can compute such crosstalk for the [PEP] configuration synthesizing the X gate, as a function of the number of modes between the computational basis and the outside mode. We can see from Fig. 4 that for a guard band of six modes (or more) the crosstalk is lower than 10^{-3} . For the synthesis in the [PEP] configuration, which had not been investigated up to now, we also compute the minimum mode spacing for which crosstalk is less than 10^{-3} between two subsequent gates. We moreover chose to target the synthesis of the least favorable gate, namely, the bit flip gate. Implementing the bit flip gate indeed requires a complete energy transfer between the two modes of the qubit, and hence a large modulation index. We obtained a minimum mode spacing of six frequency modes, similar to the [EPE] configuration to reach $\mathcal{F} \geq 0.99$. We note that a similar number of guard band modes has been found necessary to implement two Hadamard gates with a fidelity ≥ 0.99 , in the [EPE] configuration in Ref. [5].

For a computational space composed of 128 frequency modes, which we consider for this analysis, a maximum number of $\frac{128}{8} = 16$ qubit gates can thus be implemented in parallel for both [EPE] and [PEP] configurations with high performance (high fidelity and success probability).

B. Time encoding

In Sec. IV B, we showed that we were able to find the settings of the three components to synthesize with unit fidelity and success probability an arbitrary quantum gate for a single qubit encoded over two modes. The next step is to use all 128 time modes to parallelize those transformations to a maximum number of qubits, the optimal number being $M/2 = 64$ qubits.

1. Multitone rf driving of the EOM

Proposition 4. One can achieve an exact synthesis of an arbitrary unitary transformation U over all qubits with the [EPE] configuration with a square rf driving of the EOM.

Proof. The parameters have to satisfy the following set of conditions:

$$\begin{cases} |\alpha| = \cos(c/2) \\ |\beta| = \sin(c/2) \end{cases} \quad \forall k \in \llbracket 0, M/2 - 1 \rrbracket, \begin{cases} \phi_{1,k} = \frac{-d}{2} - \pi/4 \pmod{\pi} \\ \phi_{2,k} = \frac{-b}{2} + \pi/4 \pmod{\pi} \\ \phi_{1,k+M/2} = -\phi_{1,k} \pmod{\pi} \\ \phi_{2,k+M/2} = -\phi_{2,k} \pmod{\pi} \end{cases} \quad (39)$$

which implies that the phases of the EOM are independent of time on the whole interval $[0, \frac{T}{2}] = [0, \frac{\pi}{\Omega}]$: The driving signal of the EOM must then be of the form

$$x(t) = \mu \sum_{n=0}^{\infty} \frac{1}{2n+1} \sin[(2n+1)(\Omega t + \theta)], \quad (40)$$

with $\mu = 1$ and $0 < \theta < 2\pi/M$. \blacksquare

Although an infinite-sum square function allows arbitrary synthesis over all qubits, the practical implementation of such a signal is limited by the pass band of the EOM and we consider therefore more realistic cases:

(1) The ideal square function can be truncated at order N ,

$$x(t) = \mu \sum_{n=0}^N \frac{1}{2n+1} \sin[(2n+1)(\Omega t + \theta)]. \quad (41)$$

(2) The truncated function can be optimized by using different modulation index μ and modulation phase θ for each frequency component,

$$x(t) = \sum_{n=0}^N \frac{\mu_n}{2n+1} \sin[(2n+1)(\Omega t + \theta_n)]. \quad (42)$$

(3) The rf driving can be limited to a single frequency or very few frequency components, as will be considered in the next sections.

For our numerical optimizations of the parallelization of gate synthesis, we use the fidelity and success probability acceptance thresholds

$$\mathcal{F}_{th} = 0.99, \quad \mathcal{P}_{th} = 0.9999. \quad (43)$$

$$|\alpha| = 1; \quad |\beta| = 0$$

$$\forall k \in [0, M/2 - 1] \quad \phi_{1,k} + \phi_{2,k} = \frac{\nu}{2} \pmod{2\pi}$$

$$\forall k \in [0, M/2 - 1] \quad \phi_{1,k+M/2} + \phi_{2,k+M/2} = -\frac{\nu}{2} \pmod{2\pi}$$

$$\phi_{c_1} + \phi_{c_2} + \gamma = -\frac{\nu}{2} \pmod{2\pi}. \quad (45)$$

As $\phi_{i,k+M/2} = -\phi_{i,k}$, we need only write

$$|\alpha| = 1; \quad |\beta| = 0$$

$$\forall k \in [0, M/2 - 1] \quad \phi_{k,1} + \phi_{k,2} = \mu_1 \sin\left(\frac{2k\pi}{M} + \theta_1\right) + \mu_2 \sin\left(\frac{2k\pi}{M} + \theta_2\right) = \frac{\nu}{2} \pmod{2\pi}$$

$$\phi_{c_1} + \phi_{c_2} + \gamma = -\frac{\nu}{2} \pmod{2\pi}. \quad (46)$$

Figure 5 shows the number of parallel Hadamard gates above the fidelity threshold as a function of the number of frequency tones in the rf driving signal of the EOM for both [EPE] and [PEP] configurations. Considering 64 time-bin qubits, parallel synthesis of 28 almost ideal Hadamard gates can be performed, in the single-tone regime. We mean by this that the parallel synthesis of Hadamard gates can be performed with $>99\%$ fidelity and >0.9999 success probability, for up to 28 pairs of time modes. This parallelization can be brought to 47 qubits with two tones, and 53 qubits with three tones. This positions spectral LOQC as a possible platform to conduct quantum metrology experiments where a large number of quantum modes must be manipulated to achieve better precision.

In the following sections, we derive the number of parallel transformations above a given performance threshold for the Hadamard and phase gates with a single-tone rf driving of the EOM.

2. Single-tone rf driving of the EOM

Phase gates. The matrix of phase gates is of the form

$$\mathcal{M} = \begin{pmatrix} 1 & 0 \\ 0 & e^{-i\nu} \end{pmatrix}. \quad (44)$$

From the expression of the W_k matrix corresponding to the [EPE] (red) and [PEP] (blue) configuration [see Eq. (34)], we derive a set of conditions on the component parameters for the parallelization, first for the [EPE] configuration

The two modulators act as one. It is then sufficient to consider only one modulator. We can write the previous set of equations as

$$\begin{aligned} |\alpha| &= 1; \quad |\beta| = 0 \\ \forall k \in [0, M/2 - 1] \quad \phi_k &= \mu \sin\left(\frac{2k\pi}{M} + \theta\right) = \frac{\nu}{2} \pmod{2\pi} \\ \phi_c + \gamma &= -\frac{\nu}{2} \pmod{2\pi}. \end{aligned} \quad (47)$$

In the same way, conditions can be found on the component parameters for the [PEP] configuration,

$$\begin{aligned} |\alpha_1| &= |\alpha_2| = 1; \quad |\beta_1| = |\beta_2| = 0 \\ \forall k \in [0, M/2 - 1] \quad \phi_k &= \mu \sin\left(\frac{2k\pi}{M} + \theta\right) = \frac{\nu}{2} \pmod{2\pi} \\ \phi_c + \gamma_1 + \gamma_2 &= -\frac{\nu}{2} \pmod{2\pi}. \end{aligned} \quad (48)$$

or

$$\begin{aligned} |\alpha_1| &= |\alpha_2| = 0; \quad |\beta_1| = |\beta_2| = 1 \\ \forall k \in [0, M/2 - 1] \quad \phi_k &= \mu \sin\left(\frac{2k\pi}{M} + \theta\right) = -\frac{\nu}{2} \pmod{2\pi} \\ \phi_c + \gamma_1 + \gamma_2 &= -\frac{\nu}{2} \pmod{2\pi}. \end{aligned} \quad (49)$$

These three sets of equations lead to the same synthesized matrix and therefore to the same formula for the fidelity. The fidelity of each qubit k undergoing a phase change ϕ_k can be computed with the parameters for phase gates using Eq. (15) as

$$\forall k \in [0, M/2 - 1] \quad \mathcal{F}_k = \cos^2\left(\phi_k - \frac{\nu}{2}\right). \quad (50)$$

Each qubit will not realize the gate with the same fidelity, as this fidelity depends on the value of the phase at each time k . We now compute the maximum number of qubits realizing the transformation with a fidelity better than a threshold \mathcal{F}_{th} .

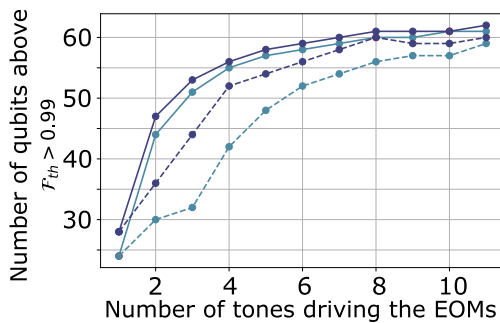


FIG. 5. Parallel Hadamard gate synthesis in time encoding framework: number of qubits above fidelity threshold $\mathcal{F}_{th} = 0.99$ as a function of the number of frequency components of the rf driving of the EOM, for the Hadamard transformation in [EPE] (light blue) and [PEP] (dark blue) configurations with exact (dotted line) and optimized (full line) truncation of a square rf driving. For time domain manipulation, the qubit space is stable, with a success probability of 100%, hence always above threshold.

For each qubit k ,

$$\mathcal{F}_k \geq \mathcal{F}_{th} \Rightarrow \cos^2\left(\phi_k - \frac{\nu}{2}\right) \geq \mathcal{F}_{th}. \quad (51)$$

Solving this equation and replacing ϕ_k by its expression, we find

$$\begin{aligned} \frac{\nu}{2} - \arccos(\sqrt{\mathcal{F}_{th}}) &\leq \mu \sin\left(\frac{2\pi k}{M} + \theta\right) \\ &\leq \frac{\nu}{2} + \arccos(\sqrt{\mathcal{F}_{th}}). \end{aligned} \quad (52)$$

The maximum value that the sine can take is bounded by the upper bound. We thus set the modulation index to this upper bound $\mu = \frac{\nu}{2} + \arccos(\sqrt{\mathcal{F}_{th}})$. Equation (52) can then be rewritten as a condition on k :

$$\begin{aligned} \frac{M}{2\pi} \arcsin\left(\frac{\frac{\nu}{2} - \arccos(\sqrt{\mathcal{F}_{th}})}{\frac{\nu}{2} + \arccos(\sqrt{\mathcal{F}_{th}})}\right) - \theta \\ \leq k \leq \frac{M}{2} - \frac{M}{2\pi} \arcsin\left(\frac{\frac{\nu}{2} - \arccos(\sqrt{\mathcal{F}_{th}})}{\frac{\nu}{2} + \arccos(\sqrt{\mathcal{F}_{th}})}\right) - \theta. \end{aligned} \quad (53)$$

The number \mathcal{N} of qubit k realizing the transformation with a fidelity over \mathcal{F}_{th} is thus given by

$$\mathcal{N} = \left\lfloor \frac{M}{2\pi} \left[\frac{\pi}{2} - \arcsin\left(\frac{\frac{\nu}{2} - \arccos(\sqrt{\mathcal{F}_{th}})}{\frac{\nu}{2} + \arccos(\sqrt{\mathcal{F}_{th}})}\right) \right] \right\rfloor. \quad (54)$$

The additional factor $\frac{1}{2}$ comes from the fact that we consider only half the values k , as we divide our 128 dimensional state of space in 64 two-dimensional subspaces \mathcal{N} decreases with increasing ν , showing that the limitation comes from the phase of the EOM. The result is shown in Fig. 6 for four values of the fidelity threshold.

Hadamard gates. The Hadamard gate requiring both phase change and energy splitting between the two modes of the

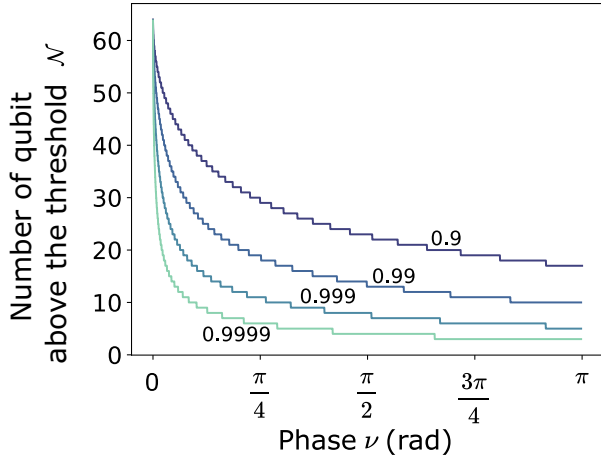


FIG. 6. Phase gates parallel synthesis: maximum number of gates synthesized in parallel with a fidelity better than \mathcal{F}_{th} for four levels of accuracy by a phase gate operating on time modes (time encoding) as a function of the required gate z -rotation angle. This dependency holds for both [EPE] and [PEP] configurations. Phase step is $\pi \times 10^{-4}$.

qubit subspace is therefore among the most difficult to synthesize.

Let us calculate the number of qubits realizing the Hadamard gate with performances exceeding \mathcal{P}_{th} and \mathcal{F}_{th} in [PEP] and [EPE] configurations: the parameters corresponding to a single Hadamard gate for qubit k are

$$|\alpha| = |\beta| = \frac{1}{\sqrt{2}}$$

$$\forall k \in [0, M/2 - 1] \quad \phi_k = \mu \sin\left(\frac{2k\pi}{M} + \theta\right) = \frac{\pi}{4} \pmod{\pi}. \quad (55)$$

By using the same method as for the phase gates, we can determine the fidelity achieved for each qubit k as

$$\forall k \in [0, M/2 - 1] \quad \mathcal{F}_k^{(EPE)} = \sin^4\left(\phi_k + \frac{\pi}{4}\right) \quad (56)$$

$$\forall k \in [0, M/2 - 1] \quad \mathcal{F}_k^{(PEP)} = \sin^2\left(\phi_k + \frac{\pi}{4}\right) \quad (57)$$

for, respectively, [EPE] and [PEP] configurations.

As for the phase gate, we look at the greater number of qubits that can realize the Hadamard transformation for [EPE] and [PEP] configurations. By starting with Eqs. (56) and (57), we find,

for the [EPE] configuration,

$$-\frac{\pi}{4} + \arcsin(\mathcal{F}_{th}^{1/4}) \leq \phi_k \leq 3\frac{\pi}{4} - \arcsin(\mathcal{F}_{th}^{1/4}), \quad (58)$$

and for the [PEP] configuration,

$$-\frac{\pi}{4} + \arcsin(\mathcal{F}_{th}^{1/2}) \leq \phi_k \leq 3\frac{\pi}{4} - \arcsin(\mathcal{F}_{th}^{1/2}). \quad (59)$$

Introducing $\Delta v_{EPE} = \frac{\pi}{2} - \arcsin(\mathcal{F}_{th}^{1/4})$ and $\Delta v_{PEP} = \frac{\pi}{2} - \arcsin(\mathcal{F}_{th}^{1/2})$, this reads

$$\frac{\pi}{4} - \Delta v_{EPE} \leq \phi_k \leq \frac{\pi}{4} + \Delta v_{EPE},$$

Maximum number of qubits realizing a given fidelity threshold for configurations PEP and EPE

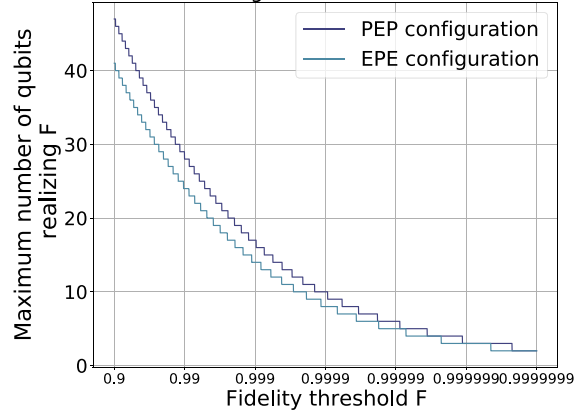


FIG. 7. Number of qubits with fidelity above threshold as a function of fidelity threshold for [EPE] (light blue) and [PEP] (dark blue) configurations with a single-frequency rf modulation.

$$\frac{\pi}{4} - \Delta v_{PEP} \leq \phi_k \leq \frac{\pi}{4} + \Delta v_{PEP}. \quad (60)$$

Similarly to the phase gate calculation, we find the maximum number of qubits achieving the Hadamard transformation with a fidelity over \mathcal{F}_{th} for both configurations:

$$\mathcal{N}_{EPE} = \frac{M}{\pi} \left[\frac{\pi}{2} - \arcsin\left(\frac{\pi}{4} - \Delta v_{EPE}\right) \right] + 1;$$

$$\mathcal{N}_{PEP} = \frac{M}{\pi} \left[\frac{\pi}{2} - \arcsin\left(\frac{\pi}{4} - \Delta v_{PEP}\right) \right] + 1. \quad (61)$$

Proposition 5. For the Hadamard gate, the number of qubits realizing \mathcal{F}_{th} is larger in the [PEP] configuration than in the [EPE] configuration for any finite number of frequencies in the rf driving.

Proof. Let $k \in [0, M/2 - 1]$ and \mathcal{F}_{th} be a fidelity threshold.

$$\mathcal{F}_k \geq \mathcal{F}_{th} \Leftrightarrow \phi_k \in \left[\frac{\pi}{4} - \Delta v, \frac{\pi}{4} + \Delta v \right]. \quad (62)$$

In the [EPE] configuration, $\Delta v_{EPE} = \frac{\pi}{2} - \arcsin(\mathcal{F}_{th}^{1/4})$.

In the [PEP] configuration, $\Delta v_{PEP} = \frac{\pi}{2} - \arcsin(\mathcal{F}_{th}^{1/2})$. ■

$$\Delta v_{PEP} \geq \Delta v_{EPE}.$$

Figure 7 indeed shows that the configuration [PEP] gives slightly better results than [EPE] for parallelization of the Hadamard gate. It is noteworthy that the number of parallel phase gates corresponding to $v = \pi/2$ is 28, as in the case of the Hadamard gate, suggesting that the performance limitation for the [PEP] configuration does not depend on the energy exchanges required by the gate but only on the required dephasing.

Table II summarizes the main results on parallelization, showing a clear advantage of time encoding over frequency encoding. This advantage of time encoding mainly comes from the two-scattering property (see Prop. 1) that can be used with the PS in the time basis, while it is not readily possible (under realistic rf bandwidth constraint) to use the EOM in the frequency basis without coupling to frequency modes

TABLE II. Comparison of the possibilities of arbitrary unitary synthesis with [EPE] and [PEP] different configurations and for two kinds of encoding. \mathcal{N} stands for the number of parallel qubits for which the gate fidelity and success probability are above threshold. The bold part corresponds to results reported in this work. Here, $\mathcal{N}_{X(H)}$ designate the number of bit flip (Hadamard) transformation that can be parallelized.

Arbitrary unitary synthesis : parallelization for $M = 128$ modes, 64 qubits		
Config.	Frequency encoding $\{\omega_j, \omega_{j+1}\}$	Time encoding $\{t_k, t_{k+M/2}\}$
[EPE]	$\mathcal{N} = 16$	\mathcal{N} with: $\mathcal{F} > 0.99, \mathcal{P} = 1$
Driving at Ω	Phase gate : $\mathcal{F} = 1, \mathcal{P} = 1$ H gate : $\mathcal{F} = 1, \mathcal{P} = 0.98$ Flip gate : $\mathcal{F} = 1, \mathcal{P} = 0.81$	$\mathcal{N}_x = 64$ $\mathcal{N}_H = 24$
Driving at : 2 Ω (Frequ.) 3 Ω (Time)	Success probability improved for high rotation angles	$\mathcal{N}_x = 64$ $\mathcal{N}_H = 44$
[PEP]	$\mathcal{N} = 16$	\mathcal{N} with: $\mathcal{F} > 0.99, \mathcal{P} = 1$
Driving at Ω	Phase gate : $\mathcal{F} = 1, \mathcal{P} = 1$ H gate : $\mathcal{F} = 1, \mathcal{P} = 0.60$ Flip gate : $\mathcal{F} = 1, \mathcal{P} = 0.27$	$\mathcal{N}_x = 64$ $\mathcal{N}_H = 28$
Driving at : 2 Ω (Frequ.) 3 Ω (Time)	No improvement	$\mathcal{N}_x = 64$ $\mathcal{N}_H = 47$

outside of the Hilbert space, composed here of two neighboring frequencies, thereby imposing important constraints on the achievable success probability.

VI. CONCLUSIONS AND OUTLOOK

Optimized for the telecom industry, electro-optic modulator (E) and pulse shaper (P) components perform mathematically complementary operations on multimode quantum photonic states. Their combination gives rise to an appealing and engineering-friendly platform for photonic quantum information processing. P and E can in particular be used in combination to perform S-LOQC, in which quantum information encoding as well as measurements are performed in the frequency basis [5]. Such a S-LOQC platform has the ability to leverage high-dimensional frequency encodings and has proven to be a promising approach for photonic quantum information processing [8,9].

In this work we focus on a subset of S-LOQC tasks, namely, the synthesis of an arbitrary single-qubit gate, and also the parallelization of such synthesis. We moreover extend our investigation beyond standard S-LOQC by considering time-bin encoding, in addition to frequency encoding. We give an overview of what can be achieved with the two paradigmatic minimal configurations, [PEP] and [EPE], for the processing of photonic qubits encoded either on frequency modes or on time modes, and we consider two main objectives: (i) the arbitrary unitary gate synthesis, with single-tone driving of the EOM, and (ii) the parallelization of the synthe-

sis of a large number of unitaries with close-to-unit fidelity and success probability.

Concerning objective (i), we compute the achievable fidelities and probabilities of success for arbitrary unitaries with single-tone rf driving of the EOM. Based on analytical and numerical studies, we show that time encoding allows the exact synthesis of an arbitrary single-qubit unitary transformation with both configurations, whereas frequency encoding only allows the exact synthesis of phase gates with maximal unit fidelity and success probability.

Concerning objective (ii), i.e., the parallelization, we have compared the two configurations [PEP] and [EPE] in terms of the number of qubit gates that can be synthesized in parallel with high performance, with a single setup of only three components with single- and dual-tone driving of the EOM. In the time encoding framework, where exact synthesis is achievable, we have shown that the number of qubits that can be manipulated with high fidelity and probability is always higher than for frequency domain implementation. We also demonstrate that the [PEP] configuration performs slightly better than [EPE] to manipulate a larger number of time-mode qubits. We have moreover analyzed the impact of the addition of tones on the number of gates that can be synthesized in parallel and provide practical solutions, i.e., truncation strategies of the rf signal, for high-fidelity Hadamard and phase gates acting on multiple time modes. Quantitatively, considering a system with 128 addressable modes (and hence 64 qubits, with dual-rail encoding) that can be realistically addressed in the near-term with EOM and PS, we notably exhibit, for time encoding, the possibility to perform the parallel synthesis of 28 Hadamard gates (with $>99\%$ fidelity and almost 100% success probability) with a single-tone EOM driving. We also show that this parallelization can be extended to 47 qubits with two tones, and to 53 qubits with three tones.

Our work illustrates the interesting perspectives offered by the combined use of pulse shapers and rf-driven electro-optics modulator to provide a versatile and powerful experimental platform for photonic information processing. The immediate perspective opened by this work will consist in validating experimentally the theoretical results presented in the present article. Such experimental validation will require in particular to be able to perform measurements in the time basis, which constitutes a challenge in terms of the required time resolution.

Considering the orders of magnitude discussed in Sec. IID, the time resolution would need to be of a few tens of picoseconds to perform a single-qubit gate in the time basis. Such resolution cannot be directly achieved using standard avalanche single-photon detectors, but time-resolved detection at the picosecond timescale is possible using superconducting nanowires [27], or by resorting to nonlinear effects [28]. On the other hand, parallel synthesis of single-qubit gates with time encoding would be limited by such time resolution. For instance, considering a time resolution of 1 ps, which is the state of the art for the jitter of the detectors, the parallelization is limited to about 10 qubits (out of 64).

Another challenge will consist in designing experimental platforms operating over a large number of modes. We assumed a number of modes $M = 128$ in the article, consistent

with what is achievable with existing technology, and notably with pulse shaper frequency resolution. Leveraging the possibility to integrate electro-optic phase modulators and pulse shapers onto photonic chips [29–32], we can moreover expect to see a sharp increase in the number of addressable modes M in the future, thereby boosting the information processing capabilities of such a platform.

Performing quantum tomography typically requires the ability to perform arbitrary single-qubit transformation followed by a measurement, and to parallelize such operation over a large number of qubits. The [PEP] and [EPE] combinations considered in this article hence appear as an appealing experimental platform for quantum tomography over qubits, and could be extended to qudits, with potential applications to the characterization of optical sources [33] or optical devices [34]. This platform can more generally be used to perform a high-dimensional Fourier transform [35,36], which constitutes a central element in boson sampling or quantum metrology experiments. As seen in Sec. IV B, the [PEP] configuration used with time-encoded qubits indeed behaves as a linear interferometer that could, for instance, be used for quantum state engineering [37], but also for optical interferometry with quantum-enhanced precision [38]. Our work highlights the relevance of considering time encoding to operate a quantum frequency processor composed of electro-optic modulators and pulse shapers. We have indeed shown that time-bin encoding enables the manipulation of a large number of qubits with high fidelity and high success probability and in general better performance than the frequency encoded versions. This work hence further positions the quantum frequency processor, which can readily leverage off-the-shelf devices at low loss telecom wavelength, as a promising contender for multimode quantum information processing.

ACKNOWLEDGMENTS

This work has been supported by Region Ile-de-France in the framework of DIM SIRTEQ, and has also benefited from the support of Telecom Paris Alumni.

APPENDIX A: GENERALIZED EXPRESSIONS FOR COMPONENT ACTION IN THE TIME BASIS

Consider the action of a single PS in the time basis. For this, recall that in the spectral mode basis, the PS matrix has a representation of the form

$$\tilde{P} = \begin{bmatrix} 1 & 0 & \dots & 0 \\ 0 & e^{i\varphi_1} & \dots & 0 \\ \vdots & \vdots & \ddots & \vdots \\ 0 & 0 & \dots & e^{i\varphi_{M-1}} \end{bmatrix}, \quad (\text{A1})$$

where $\varphi_1, \dots, \varphi_{M-1}$ denote the real phases applied to the frequency modes. The equivalent expression in the time basis is

$$\tilde{P} = FPF^\dagger = \frac{1}{M} \begin{bmatrix} 1 & 1 & 1 & \dots & 1 \\ 1 & \xi & \xi^2 & \dots & \xi^{(M-1)} \\ 1 & \xi^2 & \xi^4 & \dots & \xi^{2(M-1)} \\ \vdots & \vdots & \vdots & \ddots & \vdots \\ 1 & \xi^{(M-1)} & \xi^{2(M-1)} & \dots & \xi^{(M-1)^2} \end{bmatrix}$$

$$\begin{aligned} & \times \begin{bmatrix} 1 & 0 & 0 & \dots & 0 \\ 0 & e^{i\varphi_1} & 0 & \dots & 0 \\ 0 & 0 & e^{i\varphi_2} & \dots & 0 \\ \vdots & \vdots & \vdots & \ddots & \vdots \\ 0 & 0 & 0 & \dots & e^{i\varphi_{M-1}} \end{bmatrix} \\ & \times \begin{bmatrix} 1 & 1 & 1 & \dots & 1 \\ 1 & \xi^{-1} & \xi^{-2} & \dots & \xi^{-(M-1)} \\ 1 & \xi^{-2} & \xi^{-4} & \dots & \xi^{-2(M-1)} \\ \vdots & \vdots & \vdots & \ddots & \vdots \\ 1 & \xi^{-(M-1)} & \xi^{-2(M-1)} & \dots & \xi^{-(M-1)^2} \end{bmatrix} \\ & = \frac{1}{M} \begin{bmatrix} 1 & e^{i\varphi_1} & e^{i\varphi_2} & \dots & e^{i\varphi_{M-1}} \\ 1 & \xi e^{i\varphi_1} & \xi^2 e^{i\varphi_2} & \dots & \xi^{(M-1)} e^{i\varphi_{M-1}} \\ \vdots & \vdots & \vdots & \ddots & \vdots \\ 1 & \xi^{(M-1)} e^{i\varphi_1} & \xi^{2(M-1)} e^{i\varphi_2} & \dots & \xi^{(M-1)^2} e^{i\varphi_{M-1}} \end{bmatrix} \\ & \times \begin{bmatrix} 1 & 1 & 1 & \dots & 1 \\ 1 & \xi^{-1} & \xi^{-2} & \dots & \xi^{-(M-1)} \\ 1 & \xi^{-2} & \xi^{-4} & \dots & \xi^{-2(M-1)} \\ \vdots & \vdots & \vdots & \ddots & \vdots \\ 1 & \xi^{-(M-1)} & \xi^{-2(M-1)} & \dots & \xi^{-(M-1)^2} \end{bmatrix}, \quad (\text{A2}) \end{aligned}$$

where $\xi = e^{i(2\pi/M)}$. This expression can be expressed more compactly as

$$\forall k, k' \in [0, M-1] \quad P_{k'k} = \frac{1}{M} \sum_{j_1=0}^{M-1} \xi^{(k'-k)j_1} e^{i\varphi_{j_1}}. \quad (\text{A3})$$

The matrix of the EOM is diagonal in the time basis

$$\forall k', k'' \in [0, M-1] \quad E_{k''k'} = \delta_{k''k'} e^{i\phi_{k'}}. \quad (\text{A4})$$

The generic matrix element of the component combination [PEP] is therefore

$$\begin{aligned} (\tilde{P}E\tilde{P})_{k'k} &= \sum_j \left\{ \frac{1}{M} \sum_{j_2} \xi^{(k'-j)j_2} e^{i\varphi_{j_2}} \right\} \\ & \times e^{i\phi_j} \left\{ \frac{1}{M} \sum_{j_1} \xi^{(j-k)j_1} e^{i\varphi_{j_1}} \right\} \\ & = \frac{1}{M^2} \sum_j e^{i\phi_j} \left[\sum_{j_2} \xi^{(k'-j)j_2} e^{i\varphi_{j_2}} \right] \\ & \times \left[\sum_{j_1} \xi^{(j-k)j_1} e^{i\varphi_{j_1}} \right] \\ & = \frac{1}{M^2} \sum_{j, j_1, j_2} e^{i(\phi_j + \varphi_{j_1} + \varphi_{j_2} + \frac{2\pi}{M} [(j-k)j_1 + (k'-j)j_2])}. \quad (\text{A5}) \end{aligned}$$

The corresponding expression for the [EPE] configuration is

$$\begin{aligned}
 (E\tilde{P}E)_{k'k} &= \left\{ \sum_{k''} \delta_{k''k'} e^{i\psi_{k''}} \right\} \left\{ \frac{1}{M} \sum_j \omega^{(k''-k')j} e^{i\phi_j} \right\} \\
 &\times \left\{ \sum_k \delta_{k'k} e^{i\psi_k} \right\} \\
 &= \frac{1}{M} \sum_j e^{i\psi_{k''}} e^{i\frac{2\pi}{M}(k''-k')j} e^{i\phi_j} e^{i\psi_k} \\
 &= \frac{e^{i(\phi_k+\phi_{k'})}}{M} \sum_j e^{i\frac{2\pi}{M}(k'-k)j} e^{i\phi_j}. \quad (\text{A6})
 \end{aligned}$$

APPENDIX B: PARAMETERS OF THE PS AS A TWO-SCATTERING DEVICE IN THE TIME BASIS

We start with no assumption on the “distance” m between the two vectors of the qubit subspace

$$\forall k \in [0, M - m - 1] \quad \hat{U}_{PS}|t_k\rangle = \alpha|t_k\rangle + \beta|t_{k+m}\rangle, \quad (\text{B1})$$

where $0 < m \leq M/2$ and $(\alpha, \beta) \in \mathbb{C}^2$, $|\alpha|^2 + |\beta|^2 = 1$.

The coupling constants between time modes can be derived from the Fourier transform of the pulse shaper action in the frequency domain

$$\forall (k, k') \in \{[0, M - 1]\}^2,$$

$$P_{k',k} = \langle t_{k'} | \hat{U}_{PS} | t_k \rangle = \frac{1}{M} \sum_j \exp\left(i\frac{2\pi}{M}(k' - k)j + i\phi_j\right), \quad (\text{B2})$$

where ϕ_j is the phase applied by the PS to the frequency mode $|\omega_j\rangle$ that we want to determine for $j \in [0, M - 1]$.

Using Eq. (B1) to compute $P_{k',k}$,

$$\begin{aligned}
 \frac{1}{M} \sum_{j=0}^{M-1} e^{i\phi_j} &= \alpha \\
 \frac{1}{M} \sum_{j=0}^{M-1} e^{i2\pi\frac{mj}{M}} e^{i\phi_j} &= \beta \quad (\text{B3})
 \end{aligned}$$

$$\forall (p, q) \neq (k, k), (k + m, k), \quad \frac{1}{M} \sum_{j=0}^{M-1} e^{i2\pi\frac{(p-q)j}{M}} e^{i\phi_j} = 0.$$

Let $e^{i\phi_j} = A_j\alpha + B_j\beta$. Equation (B3) becomes

$$\begin{aligned}
 \sum_{j=0}^{M-1} A_j\alpha &= M\alpha \\
 \sum_{j=0}^{M-1} e^{i2\pi\frac{mj}{M}} B_j\beta &= M\beta. \quad (\text{B4})
 \end{aligned}$$

These equations can be satisfied by choosing $A_j = 1$ and $B_j = e^{-i2\pi\frac{mj}{M}}$, which finally gives

$$\forall j \in [0, M - 1], \quad e^{i\phi_j} = \alpha + \beta e^{-i2\pi\frac{mj}{M}}. \quad (\text{B5})$$

Then the unitarity of the PS matrix enforces the following relation:

$$\forall j \in [0, M - 1], \quad |\alpha|^2 + |\beta|^2 + 2\Re\{\alpha\beta^* e^{-i2\pi\frac{mj}{M}}\} = 1. \quad (\text{B6})$$

The case $j = 0$ imposes $\alpha\beta^*$ to be purely imaginary. Therefore, we can set $\alpha = |\alpha|e^{i\gamma}$ and $\beta = \pm i|\beta|e^{i\gamma}$, which yields a new unitarity condition

$$\forall j \in [0, M - 1], \quad \Im\{e^{-i2\pi\frac{mj}{M}}\} = 0, \quad (\text{B7})$$

which sets $m = M/2$.

It is therefore possible to choose settings of the PS so that it scatters the energy of mode $|t_k\rangle$ only into the two modes $|t_k\rangle$ and $|t_{k+M/2}\rangle$. In the frequency basis

$$\forall j \in [0, M - 1], \quad \hat{U}_{PS}|\omega_j\rangle = [\alpha + \beta e^{-i\pi j}]|\omega_j\rangle. \quad (\text{B8})$$

Finally, we obtain

$$\begin{aligned}
 \forall k \in [0, M/2], \quad \hat{U}_{PS}|t_k\rangle &= \alpha|t_k\rangle + \beta|t_{k+M/2}\rangle \\
 \forall k \in [M/2, M - 1], \quad \hat{U}_{PS}|t_k\rangle &= \beta|t_k\rangle + \alpha|t_{k-M/2}\rangle. \quad (\text{B9})
 \end{aligned}$$

Subsequently, the PS matrix takes the following form in the time basis:

$$\tilde{P}S = e^{i\gamma} \begin{pmatrix} |\alpha|I & \pm i|\beta|I \\ \pm i|\beta|I & |\alpha|I \end{pmatrix}, \quad (\text{B10})$$

where I is the identity matrix of dimension $M/2$.

- [1] H.-S. Zhong, Y.-H. Deng, J. Qin, H. Wang, M.-C. Chen, L.-C. Peng, Y.-H. Luo, D. Wu, S.-Q. Gong, H. Su *et al.*, Phase-Programmable Gaussian Boson Sampling Using Stimulated Squeezed Light, *Phys. Rev. Lett.* **127**, 180502 (2021).
 [2] J. Wang, F. Sciarrino, A. Laing, and M. G. Thompson, Integrated photonic quantum technologies, *Nat. Photonics* **14**, 273 (2020).
 [3] R. W. Boyd, *Nonlinear Optics* (Academic Press, New York, 2020).

- [4] E. Knill, R. Laflamme, and G. J. Milburn, A scheme for efficient quantum computation with linear optics, *Nature (London)* **409**, 46 (2001).
 [5] J. M. Lukens and P. Lougovski, Frequency-encoded photonic qubits for scalable quantum information processing, *Optica* **4**, 8 (2017).
 [6] H.-H. Lu, N. A. Peters, A. M. Weiner, and J. M. Lukens, Characterization of quantum frequency processors, *IEEE J. Sel. Top. Quantum Electron.* **29**, 6300112 (2023).

- [7] H.-H. Lu, J. M. Lukens, N. A. Peters, O. D. Odele, D. E. Leaird, A. M. Weiner, and P. Lougovski, Electro-Optic Frequency Beam Splitters and Tritters for High-Fidelity Photonic Quantum Information Processing, *Phys. Rev. Lett.* **120**, 030502 (2018).
- [8] H.-H. Lu, J. M. Lukens, N. A. Peters, B. P. Williams, A. M. Weiner, and P. Lougovski, Quantum interference and correlation control of frequency-bin qubits, *Optica* **5**, 1455 (2018).
- [9] H.-H. Lu, E. M. Simmerman, P. Lougovski, A. M. Weiner, and J. M. Lukens, Fully Arbitrary Control of Frequency-Bin Qubits, *Phys. Rev. Lett.* **125**, 120503 (2020).
- [10] H.-H. Lu, J. M. Lukens, B. P. Williams, P. Imany, N. A. Peters, A. M. Weiner, and P. Lougovski, A controlled-NOT gate for frequency-bin qubits, *npj Quantum Inf.* **5**, 24 (2019).
- [11] F. Samara, A. Martin, C. Autebert, M. Karpov, T. J. Kippenberg, H. Zbinden, and R. Thew, High-rate photon pairs and sequential time-bin entanglement with Si₃N₄ microring resonators, *Opt. Express* **27**, 19309 (2019).
- [12] C. Xiong, X. Zhang, A. Mahendra, J. He, D.-Y. Choi, C. Chae, D. Marpaung, A. Leinse, R. Heideman, M. Hoekman *et al.*, Compact and reconfigurable silicon nitride time-bin entanglement circuit, *Optica* **2**, 724 (2015).
- [13] H.-P. Lo, T. Ikuta, N. Matsuda, T. Honjo, and H. Takesue, Demonstration of controlled-phase gate for time-bin qubits, in *CLEO Pacific Rim Conference 2018* (Optical Society of America, 2018), p. W2G.5.
- [14] P. C. Humphreys, B. J. Metcalf, J. B. Spring, M. Moore, X.-M. Jin, M. Barbieri, W. S. Kolthammer, and I. A. Walmsley, Linear Optical Quantum Computing in a Single Spatial Mode, *Phys. Rev. Lett.* **111**, 150501 (2013).
- [15] W.-T. Fang, Y.-H. Li, Z.-Y. Zhou, L.-X. Xu, and B.-S. Shi, Towards high-capacity quantum communications by combining wavelength and time-division multiplexing technologies, in *Quantum Communications and Quantum Imaging XVI* (SPIE, Bellingham, 2018), Vol. 10771, pp. 178–183.
- [16] L. S. Madsen, F. Laudenbach, M. F. Askarani, F. Rortais, T. Vincent, J. F. Bulmer, F. M. Miatto, L. Neuhaus, L. G. Helt, M. J. Collins *et al.*, Quantum computational advantage with a programmable photonic processor, *Nature (London)* **606**, 75 (2022).
- [17] L. Orlislager, E. Woodhead, K. PhanHuy, J.-M. Merolla, P. Emplit, and S. Massar, Creating and manipulating entangled optical qubits in the frequency domain, *Phys. Rev. A* **89**, 052323 (2014).
- [18] J. Capmany and C. R. Fernández-Pousa, Quantum modelling of electro-optic modulators, *Laser Photonics Rev.* **5**, 750 (2011).
- [19] M. Tsang, Cavity quantum electro-optics. II. Input-output relations between traveling optical and microwave fields, *Phys. Rev. A* **84**, 043845 (2011).
- [20] M. A. Nielsen and I. L. Chuang, *Quantum Computation and Quantum Information*, Vol. 2 (Cambridge University Press, Cambridge, 2000), p. 23.
- [21] P. Imany, J. A. Jaramillo-Villegas, O. D. Odele, K. Han, D. E. Leaird, J. M. Lukens, P. Lougovski, M. Qi, and A. M. Weiner, 50-GHz-spaced comb of high-dimensional frequency-bin entangled photons from an on-chip silicon nitride microresonator, *Opt. Express* **26**, 1825 (2018).
- [22] P. Imany, O. D. Odele, M. S. Alshaykh, H.-H. Lu, D. E. Leaird, and A. M. Weiner, Frequency-domain Hong-Ou-Mandel interference with linear optics, *Opt. Lett.* **43**, 2760 (2018).
- [23] M. Kues, C. Reimer, P. Roztock, L. R. Cortés, S. Sciara, B. Wetzel, Y. Zhang, A. Cino, S. T. Chu, B. E. Little *et al.*, On-chip generation of high-dimensional entangled quantum states and their coherent control, *Nature (London)* **546**, 622 (2017).
- [24] A. Khodadad Kashi and M. Kues, Spectral Hong-Ou-Mandel interference between independently generated single photons for scalable frequency-domain quantum processing, *Laser Photonics Rev.* **15**, 2000464 (2021).
- [25] S. Seshadri, H.-H. Lu, D. E. Leaird, A. M. Weiner, and J. M. Lukens, Complete Frequency-Bin Bell Basis Synthesizer, *Phys. Rev. Lett.* **129**, 230505 (2022).
- [26] B.-G. Englert, C. Kurtsiefer, and H. Weinfurter, Universal unitary gate for single-photon two-qubit states, *Phys. Rev. A* **63**, 032303 (2001).
- [27] B. Korzh, Q.-Y. Zhao, J. P. Allmaras, S. Frasca, T. M. Autry, E. A. Bersin, A. D. Beyer, R. M. Briggs, B. Bumble, M. Colangelo *et al.*, Demonstration of sub-3 ps temporal resolution with a superconducting nanowire single-photon detector, *Nat. Photonics* **14**, 250 (2020).
- [28] O. Kuzucu, F. N. Wong, S. Kurimura, and S. Tovstonog, Time-resolved single-photon detection by femtosecond upconversion, *Opt. Lett.* **33**, 2257 (2008).
- [29] B. E. Nussbaum, A. J. Pizzimenti, N. B. Lingaraju, H.-H. Lu, and J. M. Lukens, Design methodologies for integrated quantum frequency processors, *J. Lightwave Technol.* **40**, 7648 (2022).
- [30] Y. Hu, M. Yu, D. Zhu, N. Sinclair, A. Shams-Ansari, L. Shao, J. Holzgrafe, E. Puma, M. Zhang, and M. Lončar, On-chip electro-optic frequency shifters and beam splitters, *Nature (London)* **599**, 587 (2021).
- [31] M. Clementi, F. A. Sabatoli, M. Borghi, L. Gianini, N. Tagliavacche, H. El Dirani, L. Youssef, N. Bergamasco, C. Petit-Etienne, E. Pargon *et al.*, Programmable frequency-bin quantum states in a nano-engineered silicon device, *Nat. Commun.* **14**, 176 (2023).
- [32] F. A. Sabatoli, L. Gianini, A. Simbula, M. Clementi, A. Fincato, F. Boeuf, M. Liscidini, M. Galli, and D. Bajoni, Silicon source of frequency-bin entangled photons, *Opt. Lett.* **47**, 6201 (2022).
- [33] H.-H. Lu, K. V. Myilswamy, R. S. Bennink, S. Seshadri, M. S. Alshaykh, J. Liu, T. J. Kippenberg, D. E. Leaird, A. M. Weiner, and J. M. Lukens, Bayesian tomography of high-dimensional on-chip biphoton frequency combs with randomized measurements, *Nat. Commun.* **13**, 4338 (2022).
- [34] V. Ansari, G. Harder, M. Allgaier, B. Brecht, and C. Silberhorn, Temporal-mode measurement tomography of a quantum pulse gate, *Phys. Rev. A* **96**, 063817 (2017).
- [35] H.-H. Lu, N. B. Lingaraju, D. E. Leaird, A. M. Weiner, and J. M. Lukens, High-dimensional discrete Fourier transform gates with a quantum frequency processor, *Opt. Express* **30**, 10126 (2022).
- [36] S. Buddhiraju, A. Dutt, M. Minkov, I. A. Williamson, and S. Fan, Arbitrary linear transformations for photons in the frequency synthetic dimension, *Nat. Commun.* **12**, 2401 (2021).
- [37] S.-H. Tan and P. P. Rohde, The resurgence of the linear optics quantum interferometer—Recent advances & applications, *Rev. Phys.* **4**, 100030 (2019).
- [38] F. Kaiser, P. Vergyris, D. Aktas, C. Babin, L. Labonté, and S. Tanzilli, Quantum enhancement of accuracy and precision in optical interferometry, *Light Sci. Appl.* **7**, 17163 (2018).